Chemical Science

Accepted Manuscript

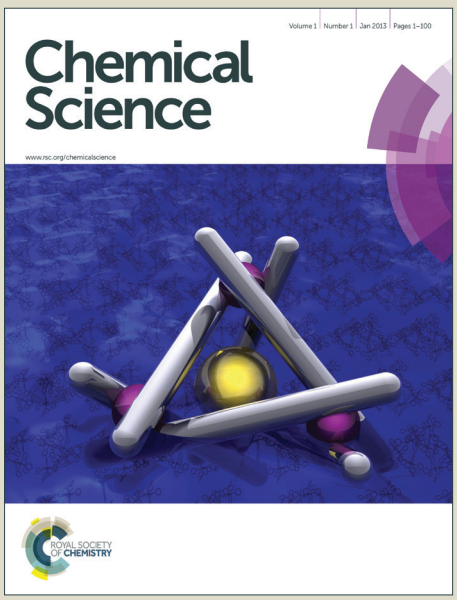

ROYAL SOCIETY OF CHEMISTRY

www.rsc.org/chemicalscience

Journal Name

RSCPublishing

ARTICLE

Interconvertible Multiple Photoluminescence Color of a Gold(I) Isocyanide Complex in the Solid State: Solvent-Induced Blue-Shifted and Mechano-Responsive Red-Shifted Photoluminescence

Cite this: DOI: 10.1039/x0xx00000x

Received 00th January 2012,
Accepted 00th January 2012

DOI: 10.1039/x0xx00000x

www.rsc.org/

Tomohiro Seki,[a] Taichi Ozaki,[a] Takuma Okura,[a] Kiyotaka Asakura,[b] Aya Sakon,[c] Hidehiro Uekusa[c]* and Hajime Ito[a]*

In this study, we report the interconvertible tetracolored solid state photoluminescence of gold(I) isocyanide complex **2** upon various external stimuli through solid state structural changes. Soaking the complex of **2** in acetone yields blue emission as a result of the formation of **2B**. The subsequent removal of acetone yields **2G** through a crystal-to-crystal phase transition, which exhibits green emission. This green-emitting solid **2G** exhibits stepwise emission color changes to yellow and then to orange upon mechanical stimulus by ball-milling, which corresponds to the formation of **2Y** and **2O**, respectively. **2B** could be recovered upon the addition of acetone to **2G**, **2Y**, and **2O**. Thus, these four emitting solid states of **2** can be switched repeatedly by means of acetone soaking and the application of mechanical stimulation. Importantly, single crystal and powder X-ray diffraction (PXRD) studies fully show the detailed molecular arrangements of **2B**, **2G**, and **2Y**. This is the first mechanochromic compound to show an interconvertible four colors emission in the solid state. We also present the first example to use PXRD measurements and the Rietveld refinement technique for the structure analysis of a ground powder in a luminescence mechanochromism study. We obtained the complete molecular-level structure information of the crystalline states of **2B**, **2G**, **2Y**, and **2O**. In comparison with a more solvophobic analogue **1**, we suggest that the weak interaction of **2** with acetone in the solid state would allow a solvent inclusion/release mode, which is an important structural factor for the unprecedented multicolor mechanochromic luminescence.

Introduction

Solid compounds that show a visible response upon mechanical stimulus have recently emerged as an interesting smart material. Mechanical stimulus, typically grinding or shearing, induces a luminescence or color change of the solid compounds, which is referred to as mechanochromism.[1] These materials are promising in sensory and recording applications. Further development of smarter functions, such as multicolor mechanochromism with a detailed understanding of the relationship between structure and optical property, is desirable. Most luminescent mechanochromic compounds show a single-step phase change upon application of a mechanical force, and there have only been a few reports of materials exhibiting dual emission color changes upon mechanical stimulation. Kato reported a brightly tricolored mechanochromic anthracene derivative which took advantage of the phase change of the liquid crystalline phase.[2] Jia reported a mechanical force strength-dependent mechanochromic molecule containing two different chromophore units, which exhibited two individual emission color changes.[3] The group of Yamaguchi and Saito found that tetrathiazolyl thiophene exhibits distinct emission color changes with a change of pressure and shearing force.[4] More recently, the Yagai and Ito group reported a rational design of a mechanochromic compound with dipolar and amphiphilic characters that showed a two-step emission color change.[5] However, solid materials that show a multiple luminescence color change are still rare. To the best of our knowledge, no mechanochromic materials that show a tetracolored luminescence change have been reported.

The luminescent properties of the molecules that show luminescent mechanochromism are very sensitive to environmental changes around the molecules and are strongly related to their solid state structures. In a typical case of luminescence mechanochromism, the crystalline structure of the mechanochromic compound is changed to an amorphous phase, which exhibits a different luminescence color from that observed in its crystalline state.[3,6] The amorphous phase can revert to the original crystalline structure through

recrystallization by solvent fuming or heating. We previously reported the first demonstration of the reversible luminescent mechanochromism of **1** based on this mechanism (Fig. 1 and 2a).[6a] The mechanical grinding or shearing is noncoherent and exerts random stimuli on the solid. Thus, these mechanical stresses tend to induce a crystalline-to-amorphous phase transition, in which the latter phase has a random structure when compared with the former. Approximately 80% of reported crystalline mechanochromic luminescent materials show this type of phase transition.[3,6] Some mechanochromic compounds co-crystalize with a solvent and yield an amorphous phase after grinding accompanied by solvent release.[7] Luminescent mechanochromism caused by conversion of one crystal structure to another with a different molecular arrangement constitutes only 10% of mechanochromic luminescent materials.[4,8] More remarkable mechanisms, such as mechano-triggered single-crystal-to-single-crystal phase transition of mechanochromic gold(I) isocyanide complexes, have been reported by our group.[9] In most examples, luminescent mechanochromism compounds can only show a single phase transition upon mechanical stimulation. Multiple phase transitions can realize multiple responses; however, such materials have been rarely reported.

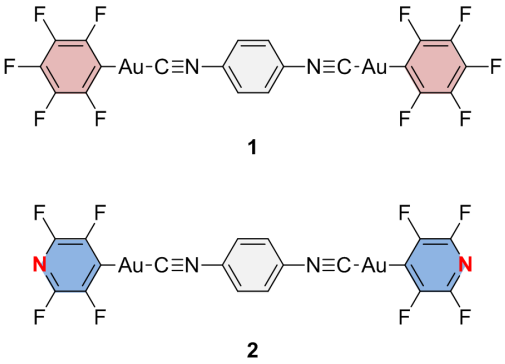

Fig. 1 Structures of gold(I) isocyanide complexes **1** and **2**.

One obstacle facing researchers for the study of mechanochromism is the difficulty in the structure analysis of the powdery solid samples obtained after the mechanical process. This is in contrast to solid structure analyses before mechanical stimulation of the sample, in which the crystalline material can be analyzed by single crystal X-ray analysis. Powder X-ray diffraction (PXRD) measurements and Rietveld refinement techniques are known to be powerful methods for crystalline structure analyses of powder materials; however, there have been no reports of this method being applied to mechanochromic materials.[10]me

In this paper, we report a new mechanochromic luminescent material **2** (Fig. 1), showing crystal-to-crystal-to-amorphous phase changes upon mechanical grinding and solvent-related structure modifications. As a result, compound **2** shows four individual solid state emissions, which are interconvertible by addition of solvent and application of mechanical force (Fig. 2b–d). We studied the optical properties and single crystal and powder X-ray diffraction analyses of the new compound **2**. For the first time, we solved the crystalline structure of ground powders of the luminescent mechanochromic compound by PXRD measurements and Rietveld refinement. Thermal analyses of **2** provide the unique profile feature of its crystalline structure change upon mechanical stimulation. Compound **2** is shown to be the first mechanochromic compound incorporating four interconvertible structures with different emission properties. The structure analysis reveals that the weak interaction between the solvent and **2** created the solvent releasing crystal-to-crystal conversion, which is an unprecedented mechanochromic structural change. The combination of two crystal-to-crystal phase changes and one crystal-to-amorphous phase change results in the novel interconversion between four different colors.

Results and Discussion

Stimuli-Responsive Emission Color Changes.

We previously reported the reversible two-colored luminescent mechanochromism of gold(I) isocyanide complex **1** exhibiting phase transition from blue-emitting **1B** to yellow-emitting **1Y** (Fig. 2a).[6a] This emission color change arises from the crystalline-to-amorphous phase transition as revealed by the PXRD pattern. We suggested that this yellow emission in the amorphous ground powder **1Y** was responsible for the formation of aurophilic interactions.[1d,e,11,12] The original blue emission was recovered upon addition of dichloromethane onto **1Y**, owing to partial dissolution followed by recrystallization. The role of dichloromethane is to facilitate recrystallization of the amorphous **1Y** to crystalline **1B**. Both **1B** and **1Y** are solvophobic and do not contain any solvent in their crystalline lattice.

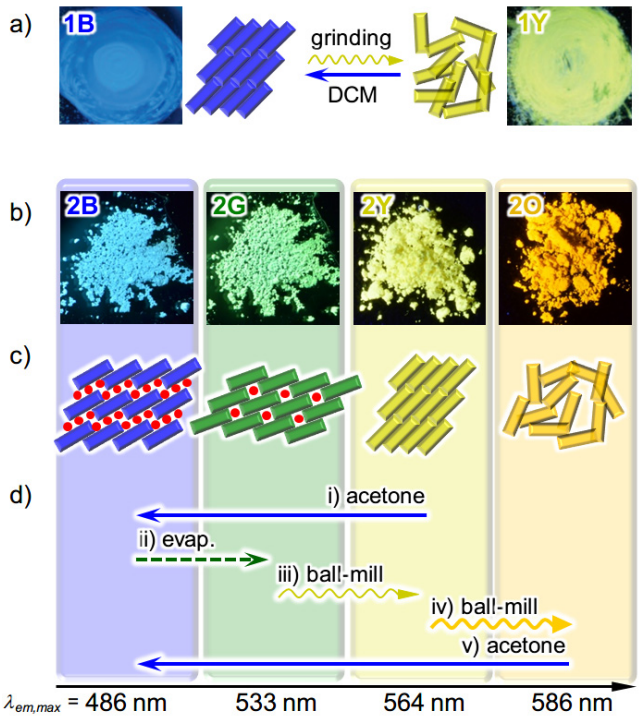

Fig. 2 a) Photographs and schematic representations of molecular arrangements of **1** showing different photoluminescence upon applying external stimuli. The molecule of **1** is denoted as a rectangle. b) Photographs of the powder forms of **2** showing different photoluminescence under UV light at 365 nm. c) Schematic representations of the solid state molecular arrangements of **2** in which a **2** molecule is denoted as rectangles with colors of the corresponding emission. Solvent molecules are denoted as red circles. d) Specific procedures for the interconversion of four emitting states of **2**.

The new complex **2** shows four individual emission colors which are interconvertible by treatment of acetone and mechanical stimuli (Fig. 2b–d). As-synthesized yellow solid of **2** exhibits yellow emission under UV light irradiation at 365 nm and thus is referred to as **2Y** (Fig. 2b). The emission color of **2Y** immediately turns into blue upon soaking the powder in acetone (step *i* in Fig. 2d and Fig. S1†), and the resulting polymorph is referred to as **2B**. It should be noted that complex **2** is scarcely soluble in acetone (c_{max} = 0.2 mg/mL) and its acetone solution is not emissive in the visible region.[13] Upon air drying of **2B**, the polymorph **2B** immediately transforms to a green-emitting polymorph **2G** (step *ii* in Fig. 2d and Fig. S1†). **2G** may contain acetone molecules in the crystal lattice, but did not show any further emission color changes even under reduced pressure for weeks. When **2G** was ground using a pestle, yellow and orange emissions were observed upon gentle and hard grinding, respectively (Fig. 2a†). After several experiments, we determined that two different solid states with distinct emissions emerge in a stepwise fashion by ball-milling with grinding over a short and long duration (Fig. 2b†). When **2G** was mechanically stimulated in a ball-mill at 4600 rpm for 10 min (short grinding), the emission color of the powder was yellow (step *iii* in Fig. 2d), indicating the recovery of **2Y**. When **2Y** is ground by ball-mill for an additional 5 min (long grinding), orange colored emission was observed, corresponding to the formation of **2O** (step *iv* in Fig. 2d). Similar mechano-responsive stepwise emission color changes have rarely been reported in the literature.[3,5] After further grinding of **2O** for 1 h, no subsequent changes in the orange emission are observed. The reversion of **2O** to **2B** occurs by soaking the powder in acetone (step *v* in Fig. 2d), indicating the interconvertibility between the four emission colors of **2**.[14] The following solid state spectroscopic studies of **2** indicate that the treatment with acetone induces crystalline structure changes with blue-shifted emission (steps *i* and *v* in Fig. 2d), whereas mechanical grinding results in those with red-shifted emission (steps *iii* and *iv* in Fig. 2d).

Optical properties of the four emitting solid states of **2** were investigated by steady-state spectroscopy (Fig. 3). Under excitation at 365 nm, all the solid materials of **2** show broad emission bands that are devoid of vibrational structure (solid lines in Fig. 3). Emission spectra of **2B**, **2G**, **2Y**, and **2O** have maxima at 486, 533, 564, and 586 nm, respectively, confirming the wide coverage of the visible spectral region. This is in contrast to the THF solution of **2** which is not emissive [absolute emission quantum yield (Φ_{em}) is 0%, Fig. 3†]. This indicates that the solid state emission properties of **2** are dependent on the aggregation in the solid phase. Excitation spectra of **2B**, **2G**, **2Y**, and **2O** detected at the emission maxima show broad bands peaked at 385, 415, 397, and 459 nm, respectively (dashed lines, Fig. 3). UV–vis absorption spectrum of the THF solution of **2** showed an absorption band at a range of 200–300 nm (Fig. 4†), shorter than the regions of the excitation bands observed for **2B**, **2G**, **2Y**, and **2O**. The different excitation spectra suggest that the ground state structures of **2B**, **2G**, **2Y**, and **2O** in the solid phases are distinct from each other.

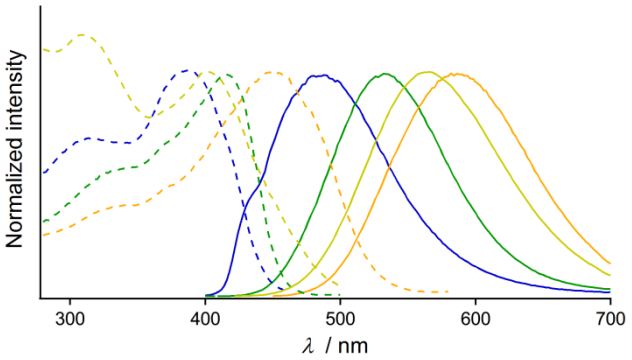

Fig. 3 Normalized excitation (dashed lines, monitored at the emission maxima) and emission spectra (solid lines, λ_{em} = 365 nm) of **2B** (blue lines), **2G** (green lines), **2Y** (yellow lines), and **2O** (orange lines).

Photophysical properties were investigated for the powders of **2** with different emission properties and the results are summarized in Table S1†. The Φ_{em} of **2B** and **2G** are both 10%, whereas Φ_{em} of **2Y** and **2O**, both obtained by ball-milling, are 27 and 30%, respectively (Table S1†). Mechanical force-induced emission color change with increased Φ_{em} was reported for organometallic complexes.[6a,9b] Photoluminescence lifetime spectroscopy was also carried out and emission decay profiles are presented in Fig. 5. The emission decay profiles of **2B**, **2G**, **2Y**, and **2O** were all fitted to a biexponential curve. The average lifetime τ_{av} [= $(\Sigma A_i\tau_i)/(\Sigma A_i)$] of **2G**, **2Y**, and **2O** are almost the same within the range of 0.4–0.7 μs (Table S1†). However, a longer τ_{av} value of 2.55 μs was observed for **2B**.

Stimuli-Responsive Crystalline Structural Changes.

PXRD measurements indicate that **2B**, **2G**, **2Y**, and **2O** have distinct packing arrangements. It has been reported that the emission properties of the solid materials are significantly related to the crystalline structures and the intermolecular interaction patterns.[15] The powders of **2B**, **2G**, and **2Y** showed several intense diffractions (Fig. 4), indicating their crystalline nature. The diffraction of **2Y**, obtained by short grinding (ball-milling for 10 min), is principally similar to that of the as-synthesized powder (Fig. 6†), consistent with the similarity in their emission. Moreover, the PXRD patterns indicate that crystalline-to-crystalline phase transition from **2G** to **2Y** occurs upon mechanical stimulation.[4,8] Unlike the above three patterns, the PXRD pattern of **2O** showed diffractions with very small intensity (orange line in Fig. 4), indicating that **2O** is in an amorphous phase. The crystalline-to-amorphous phase transition from **2Y** to **2O** is likely a result of the long grinding (ball-milling for 15 min) disrupting the ordered molecular arrangements as commonly observed for mechanochromic compounds.[3,6] Four different diffraction patterns of **2B**, **2G**, **2Y**, and **2O** indicate that each of their crystalline arrangement is distinct. As multicolored luminescent mechanochromic compounds have rarely been reported,[2-5] the relationship between their detailed crystalline structures and emission properties should give us useful insights.

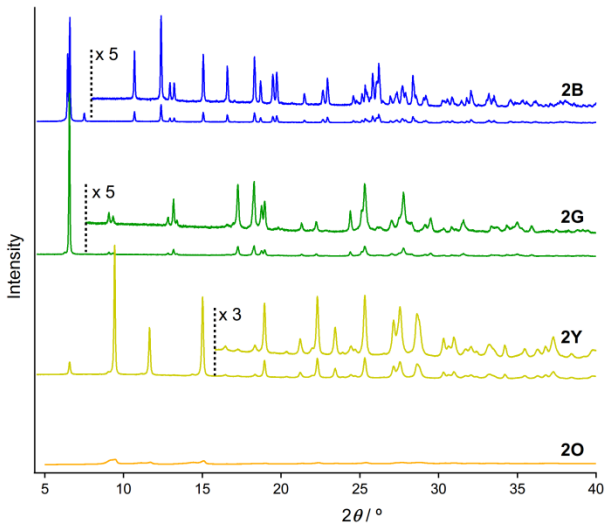

Fig. 4 PXRD patterns of **2B** (blue line), **2G** (green line), **2Y** (yellow line), and **2O** (orange line).

To gain a better understanding of the structure–property relationship of **2B**, we performed single crystal X-ray diffraction analyses. The blue-emitting single crystal was prepared from a saturated acetone solution of **2**. **2B** was crystallized as triclinic *P*-1 (Fig. 5, Table 1 and S2†). The central isocyanide benzene ring of the molecule is on the inversion center. The simulated powder pattern obtained from the single crystal structure is identical to the PXRD pattern of **2B** (Fig. 7a†). Molecules in **2B** form a layer-like structure with an interlayer spacing *d* of 13.22 Å in which the molecular tilt angle is 28.61°. For each molecule, the dihedral angle $\theta_{dihedral}$ between central benzenes and lateral pyridines is 34.03°. Within the layer, the molecules form four CH···F intermolecular interactions with the adjacent two molecules (Fig. 8†) to construct a tape-like motif. **2B** contains 2 equivalents of disordered acetone molecules which form sublayers between the tape-like structures of **2** (**2B**: [**2**] × 2 = [acetone]; Fig. 5b). The gold molecules in the tapes and the acetone molecules in the sublayers interact via CH···O and CH···F intermolecular interactions (Fig. 8†). The absence of defined intermolecular interactions between the tapes, owing to the presence of the acetone sublayers, is thought to make **2B** unstable under acetone-free conditions. The molecules in the tapes stack on top of each other without a prominent longitudinal offset through π–π stacking interactions both between benzene rings and between pyridine rings with a perpendicular distance of 3.314 and 3.334 Å, respectively. These intermolecular interactions in the tapes of **2B** may play an important role to achieve longer wavelength emission compared with that of the solution phase. However, the Au···Au distance of 3.5452(7) Å (Fig. 5a) is beyond the limit of aurophilic interactions, which indicates their negligible influence on the emission energy level of **2B**.

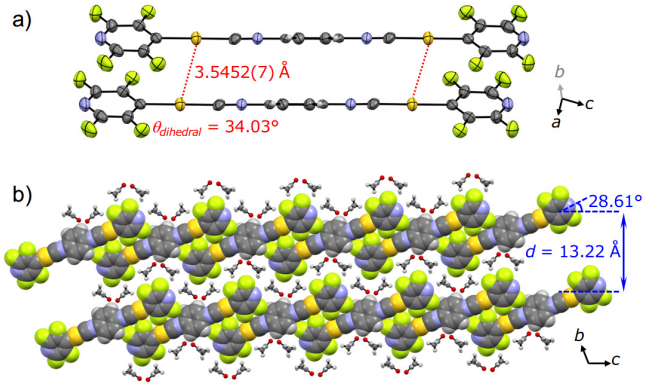

Fig. 5 a) ORTEP representation of the dimer and b) the space-filling representation of the packing structures of **2B** viewed along the direction of the *a* axis. Acetone molecules are depicted as ball-and-stick models in b).

Table 1 Summary of crystal structure analyses of **2B**, **2G**, and **2Y**.

	2B	**2G**	**2Y**
CCDC number	1035806	1035808	1035810
Specimen	Single crystal	Single crystal	Powder
Crystal system	triclinic	triclinic	monoclinic
Space group	*P*-1 (#2)	*P*-1 (#2)	$P2_1/c$ (#14)
a / Å	3.5452(4)	3.5707(3)	7.79058(18)
b / Å	14.0087(15)	10.3087(10)	18.7202(5)
c / Å	14.2490(15)	14.2742(11)	6.74157(17)
α / °	109.292(3)	107.689(4)	90
β / °	91.673(3)	92.505(5)	103.167(3)
γ / °	91.322(2)	100.205(5)	90
V / Å^3	667.23(13)	489.99(8)	957.35(5)
Z value	1	1	2
D_{calc} / g·cm^{-3}	2.335	2.786	-
R_1 / %[a]	4.73	10.08	-
wR_2 / %[b]	10.55	25.46	-
GOF[c]	1.152	1.114	-
R_{wp} / %	-	-	4.62
R_p / %	-	-	3.60
R_{F2} / %	-	-	2.74

[a]: For data with $I > 2.00\sigma(I)$. [b]: For all reflection data. [c]: Goodness of Fit.

The single crystal X-ray diffraction analysis of **2G** provides information on the origin of the emission color change. For preparation of the single crystal **2G**, single crystal **2B** was exposed either to air or water vapor to remove the incorporated acetone molecules. The resulting green-emitting crystals obtained by both methods afforded the similar packing structures and the latter method yielded better diffraction data. Both methods are observed to yield **2G** because their simulated powder patterns are identical to the PXRD pattern of **2G** (Fig. 7b†). **2G** is crystallized into the triclinic space group *P*-1 (Fig. 6, Table 1 and S2†). The central isocyanide benzene ring of the molecule is on the inversion center. **2G** forms layered structures (Fig. 6b) similar to **2B**. The layer spacing *d* of **2G** is 9.821 Å in

which the molecular tilt angle is 21.66°. In **2G**, a 1-D channel structure with some residual electron density along the *a* axis exists between the molecular tape structures (Fig. S9a†), indicating the inclusion of a small amount of acetone molecules. Based on the X-ray diffraction analyses and ^{1}H NMR spectroscopy, the included acetone molecules in **2G** are less than 0.5 equivalents (**2G**: [**2**] × *n* = [acetone], *n* < 0.5).[16] Owing to the lack of an "acetone sublayer" in **2G**, the gold complexes in the tape structure **2G** can interact with adjacent complexes through multipoint F···F and CH···F interactions (Fig. S9b†). As a result, flat 2-D sheets which extend along the *bc*-planes are formed. Between sheets, molecules stack on top of each other without offset through π–π stacking interactions with a perpendicular distance of 3.509 Å (benzene rings) and 3.330 Å (pyridine rings). **2B** does not contain aurophilic interactions [Au···Au separation: 3.571(2) Å] (Fig. 6a). Smaller excitation energy of **2G** compared with that of **2B** may be caused either by smaller amounts of solvent inclusion, which may enhance chromophore–chromophore interactions, or by the rather flat conformations of the chromophore ($\theta_{dihedral}$ = 11.92°), which may lead to an effective intra- and/or intermolecular conjugation.[17]

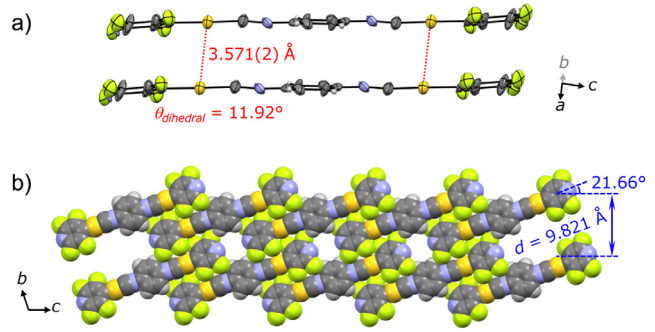

Fig. 6 a) ORTEP representation of the dimer viewed along roughly to the direction of *b* axis and b) space-filling representation of packing structures of **2G** viewed along the direction of the *a* axis.

PXRD measurements and Rietveld refinement disclosed detailed crystalline structure of **2Y** demonstrating that its yellow emission is caused by aurophilic interactions. The molecular packing arrangement of **2Y** was determined with a suitable quality from PXRD data with a range of 2θ = 7–60° (Fig. S10†).[18] It should be noted that the present study is the first example showing the great advantage of *ab initio* structural analyses of ground powders of mechanochromic compounds.[19] Ground powder **2Y** crystallizes in the monoclinic space group $P2_1/c$ (Fig. 7 and Table 1 and S3†). The central isocyanide benzene ring of the molecule is on the inversion center. The molecular packing arrangement of **2Y** is rather different from those of **2B** and **2G**. For example, no solvent molecules exist in the crystalline lattice of **2Y**, which is also supported by thermal analyses, elemental analyses and ^{1}H NMR spectroscopy (Fig. 8 and S13 and Table S4†). Moreover, face-to-face stacking of the molecules is absent. Instead, infinite chains of Au···Au interactions with a distance of 3.428(2) Å are formed along the direction of the *c* axis (Fig. 7a). This distance is within the range of aurophilic interactions, and is likely to be responsible for the emission property of **2Y** with a low excited energy level. Perpendicular to the aurophilic bond, molecules afford a flat sheet through multipoint F···F interactions between the tape-like motif (Fig. S11a†). Within the sheet, all the molecular long axes are oriented along the same direction, and in the adjacent sheet molecules are oriented at approximately 90° with respect to those in the next layer (Fig. S11b†). This is the first report of the mechano-induced crystal-to-crystal phase conversion with solvent release.

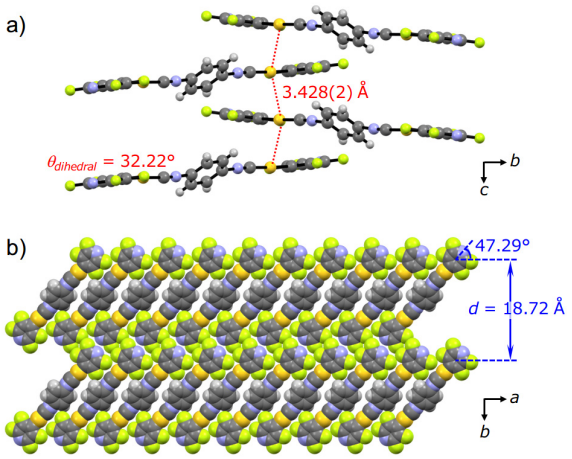

Fig. 7 a) Ball-and-stick representation of the tetramer viewed along the direction of the *a* axis, and b) the space-filling representation of the packing structures of **2Y** viewed along the direction of the *c* axis.

Orange emission of **2O** with the smallest excitation energy in the four different structures of **2** would be attributed to the aurophilic bonds with the shortest Au···Au distance. Owing to the amorphous nature, the detailed intermolecular interaction patterns existing in **2O** are unclear. TGA, elemental analyses and ^{1}H NMR spectrum revealed that **2O** contains no solvent molecules (Fig. 8 and S14 and Table S4†), therefore chromophore–chromophore interactions, rather than chromophore–solvent interactions, must be involved. From the longest wavelength maxima in the excitation and emission spectra, it is more likely that aurophilic interactions with shorter Au···Au separation compared with those observed in **2Y** should be present.[6a] In the amorphous ground phase of mechanochromic organometallic compounds, it is reported that metallophilic bonds are formed that effect its emission properties.[6a,b,7e,g]

The above discussion indicates that **2** can form two solvated (**2B** and **2G**) and two non-solvated solid states (**2Y** and **2O**). This can be confirmed by the experimental results of the crystal structure analyses, thermal analyses, elemental analyses and ^{1}H NMR spectroscopy as mentioned above (see the Electronic Supplementary Information). This is further supported by the IR spectroscopy: IR spectra of **2B** and **2G** show carbonyl stretching vibrational band at around 1715 cm^{-1}, while **2Y** and **2O** do not (Fig. S15). Therefore, the crystalline structure changes with solvent inclusion/release mode are important for interconvertible multiple photoluminescence color of **2**.

Thermal Analyses.

Thermal analyses of **2G** (Fig. 8a) reveal that its phase transition into the **2Y** phase occurs with solvent release. DSC measurement of **2G** showed the endothermic peak at 95 °C (green arrow in Fig. 8a) before observation of the prominent exothermic peaks of their decomposition above 250 °C. The endothermic peak at 95 °C can be attributed to the thermal

phase transition from **2G** to **2Y**[20] because the emission color of **2G** changed from green to yellow at this temperature (Fig. S16†). This phase transition (**2G** → **2Y**) occurs with solvent release: the TGA profile of **2G** reveals a 5% weight loss around at 90 °C (dashed line in Fig. 8a). This result suggests that the phase transition of **2G** by short grinding also induces solvent release to form **2Y**.[21] Although mechanochromism with solvent release was reported previously,[7] this is the first report of a crystal-to-crystal phase conversion.

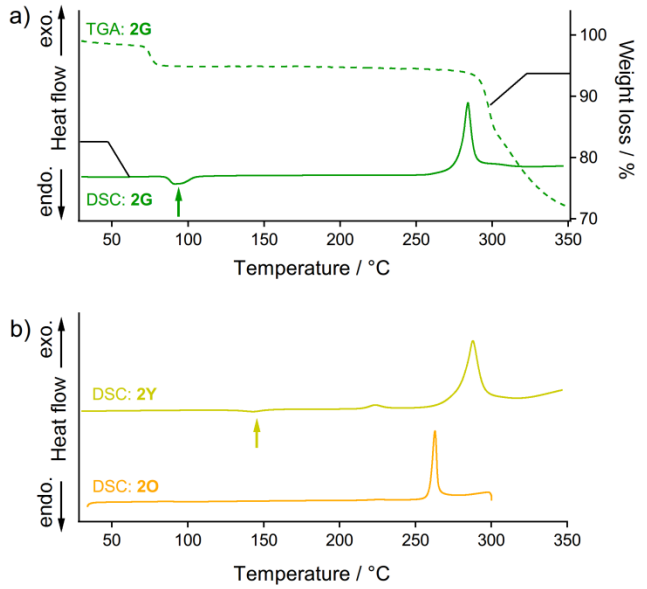

Fig. 8 a) DSC (solid line) and TGA profiles (dashed line) of **2G**. Green arrow indicates the endothermic phase transition from **2G** to **2Y**. b) DSC profiles of **2Y** (yellow line) and **2O** (orange line). Yellow arrow indicates endothermic phase transition from **2Y** to **2O**. For DSC and TGA profiles, the heating rate is 10 °C/min.

DSC analyses show the relative thermodynamic stability of solvent-free forms of **2Y** and **2O**.[22] DSC measurement of **2Y** showed the endothermic peak of the phase transitions around 145 °C (yellow arrow in Fig. 8b). The emission color change of **2Y** from yellow to orange was also observed around 160 °C upon heating treatment (Fig. S16†). Thus, the endothermic peak of **2Y** at 145 °C can be attributed to the thermal phase transition from **2Y** to **2O**. The TGA profile of **2Y** does not show any discernible weight loss in this range of temperatures, because no solvent is included (Fig. S17†). However, DSC and TGA profiles of **2O** do not show any peaks until decomposition above 250 °C (orange line in Fig. 8b and Fig. S17†), owing to the absence of the phase transition upon heating. This is supported by the fact that the thermal-induced emission color change of **2O** is absent (Fig. S16†). From these results, **2Y** can be considered as the solvent-free metastable polymorph of **2**, while **2O** is the solvent-free, thermodynamically more stable phase.[23]

The fact that the phase transition from **2G** to **2Y** requires solvent release and that **2Y** is less thermodynamically stable than **2O** is a key to realize a unique two-step mechanochromism, **2G** → **2Y** → **2O** (steps *iii* and *iv* in Fig. 2d). In the initial stage of grinding of **2G** (step *iii* in Fig. 2d), included solvent molecules start to be released owing to decreasing the particle size and increasing the surface area of the solid sample. This initiates molecular rearrangement of **2G** to form the solvent-free forms. As a result, **2Y** is initially formed as a kinetically trapped metastable intermediate. Additional mechanical stimulation provides **2O** phase (step *iv* in Fig. 2d), which is the more thermodynamically stable form of **2**. This type of crystal-to-amorphous phase transition (**2Y** → **2O**) upon mechanical stimulation in a solvent-free solid state condition is most commonly observed for mechanochromic compounds.[3,6] As mentioned above, we confirm that **2B** and **2G** contain solvent molecules in their crystalline lattices while **2Y** and **2O** do not contain any solvent molecules based on crystal structure analyses, thermal analyses, elemental analyses and ^{1}H NMR and IR spectroscopy (see the Electronic Supplementary Information).

Role of tetrafluoropyridyl groups on unique stimuli-responsivity of 2.

It is surprising that substitution of the pentafluorophenyl group in **1** by a tetrafluoropyridyl group in **2** leads to a dramatic enhancement of its stimuli-responsivity (Fig. 2). It has been reported that subtle modification of chemical structure can induce a significant change in solid state structures.[15] As the overall crystalline structures are generally determined by accumulation of relatively weak intermolecular interactions, it is sometimes difficult to understand relationships between molecular and crystalline structures. Indeed, at this stage, it is difficult to fully determine which molecular structural factor of **2** is important for its unique stimuli-responsivity.†

However, one possible explanation about the impact of the molecular structure on the mechanochromic property concerns the relatively high polarity of **2** (Fig. S17†), which may help the formation of the weak interaction with acetone. For the previously reported solvophobic complex **1** containing a C_6F_5 moiety, the molecules in the crystals were densely packed, and no solvent inclusion was observed.[6a] Complex **2** with a C_5NF_4 moiety is more polar and less solvophobic compared with **1**. This enables the solvent inclusion/release process owing to the weak interactions between the polar molecule **2** and acetone. In the presence of many solvent molecules, blue-emitting **2B** was formed, then after evaporation of the acetone, the less solvated **2G** was formed. As the solvated acetone molecules were weakly absorbed in the crystal lattice, the weak mechanical stimulation induces the solvent release to produce non-solvated **2Y**. The slight molecular structure change from **1** with the C_6F_5 moiety to less solvophobic **2** with the C_5NF_4 moiety is an important key factor to realize unprecedented crystal-to-crystal-to-amorphous phase transition with the different emission color changes.

Conclusions

We report complex **2** which can take four different solid state structures with different emission properties. These four different emissions of **2** in the solid state are reversible. This multiple switching of the solid state emission of **2** was caused by a combination of dual two-step emission color changes which are induced by solvent inclusion/release and short/long mechanical stimulation. In an acetone atmosphere, the blue-emitting **2B** was formed, and after acetone release, the green-emitting **2G** was formed. Upon applying mechanical stimulus to **2G**, two-step emission color changes to yellow (short ball-milling) and then to orange (long ball-milling) were observed, which correspond to phase changes into **2Y** and **2O**, respectively. Single crystal and powder X-ray diffraction

analyses successfully revealed all the detailed molecular arrangements of **2B**, **2G**, **2Y**, and **2O**. We found that both **2B** and **2G** formed solvated crystalline structures without defined aurophilic interactions. Conversely, **2Y** powder formed solvent-free ordered molecular arrangement involving aurophilic interaction. The amorphous **2O** phase is suggested to contain aurophilic interaction with the shortest Au···Au distance. Thermal analyses revealed that the phase transition from **2G** to **2Y** requires solvent release. Moreover, the amorphous **2O** phase is thermodynamically more stable than the **2Y** phase. Thus, this unique two-step mechanochromism (**2G** → **2Y** → **2O**) upon mechanical stimulation starts with solvent release from **2G** followed by rearrangement into solvent-free **2Y** (crystal-to-crystal phase transition), and then crystal-to-amorphous phase transition takes place to form the thermodynamically more stable **2O**. Comparison between **1** with a C_6F_5 moiety and **2** with a C_5NF_4 moiety suggests that the more polar and less solvophobic nature of **2** may create the solvent inclusion/release structure transition. This is an important factor for the multiple structures and emission color transformation of **2**. The present multicolored mechanochromic complex **2** with fully-solved structures can be considered as a new type of smart material.

Experimental section

Synthesis of 2,3,5,6-tetrafluoropyridyltetrahydrothiophene)gold(I):

2,3,5,6-tetrafluoropyridine (755.3 mg, 5.0 mmol) was dissolved in dry THF (20 mL) with stirring at –78 °C in a 100-mL round-bottomed flask, then *n*-BuLi (1.65 M hexane) was added dropwise for 15 min. After 1 h, chloro(tetrahydrothiophene)gold(I) (1.92 g, 6.0 mmol) was added to the reaction mixture. Then, the mixture was allowed to warm to room temperature and stirred for 1 h. Addition of a small portion of water quenches the reaction. $MgSO_4$ was added to the mixture and stirred for 20 min. $MgSO_4$ was filtered off by filtration and solvent was evaporated. The residue was quickly passed through a short silica gel column (CH_2Cl_2/hexane = 50:50, 100 mL) to give the white-purple solid. ^{1}H NMR (400 MHz, $CDCl_3$, δ (ppm)): 2.24 (s, 4H), 3.46 (s, 4H). ^{13}C NMR (100 MHz, $CDCl_3$, δ (ppm)): 30.7 (*C*H_2), 38.7 (*C*H_2), (*C*H), 141.7 (*C*H), 143.9 (*C*H), 144.3 (*C*H). HRMS-FAB (m/z): [M+H] calcd for $C_{19}H_9AuNF_4^+$, 436.0052; found, 436.0058. Anal. Calcd for $C_{19}H_8AuNF_4$: C, 24.84, H, 1.85; N, 3.22. Found: C, 24.87; H, 1.90; N, 3.05.

Synthesis of 2,3,5,6-tetrafluoropyridyltetrahydrothiophene)gold(I):

A mixture of 1,4-diisocyanobenzene (64.1 mg, 0.5 mmol) and 2,3,5,6-tetrafluoropyridyl(tetrahydrothiophene)gold(I) (435.2 mg, 1.0 mmol) in CH_2Cl_2 (5 mL) was stirred for 30 min under a N_2 atmosphere at room temperature. The precipitates were filtered and washed with CH_2Cl_2, and dried in *vacuo* to obtain **2** as a yellow solid (350.3 mg, mmol, 85%). ^{1}H NMR (400 MHz, THF-d_8, δ (ppm)): 8.14 (s, 4H). The poor solubility of **2** in solvents hampered ^{13}C NMR measurements. HRMS-FAB (m/z): [M+H] calcd for $C_{18}H_5Au_2N_4F_8^+$, 822.9712; found, 822.9711. Anal. Calcd for $C_{18}H_4Au_2N_4F_8$: C, 26.30, H, 0.49; N, 6.81. Found: C, 26.23; H, 0.64; N, 6.63.

Preparation of 2B:

The blue luminescent powder **2B** is prepared from **2Y**, **2G**, and **2O** immediately after they are soaked in acetone. IR (neat): $\tilde{\nu}$ = 2218, 1704, 1628, 1543, 1421, 1214, 927, 832 cm^{-1}.

Preparation of 2G:

Upon air drying a powder of **2B** to evaporate acetone, green-emitting **2G** is immediately formed. IR (neat): $\tilde{\nu}$ = 2209, 1628, 1453, 1207, 929, 838 cm^{-1}. ^{1}H NMR [400 MHz, THF-d_8, Fig. S12, δ (ppm)]: 8.14 (s, 4H). Methyl proton of included acetone was also observed at 2.11 ppm. Anal. Calcd for $C_{18}H_4Au_2N_4F_8$: C, 26.30, H, 0.49; N, 6.81. Found: C, 26.67; H, 0.89; N, 6.63.

Preparation of 2Y:

As-prepared solid **2Y** is analytically pure but, in terms of the crystalline arrangement, it is impure as shown by PXRD pattern (Fig. S6). For purification of as-synthesized **2Y**, **2** was suspended in cyclohexanone (c_{max} = 1 mg/mL) and filtered and washed with that solvent, then dried in *vacuo* to give the yellow-emitting powder **2Y**. Alternative preparation method of **2Y** is to grind **2G** in a ball-mill at 4600 rpm for 10 min (Taitec Bead Crusher μT-01). Typically, **2G** (50 mg) and a stainless bead (1/8 inch) were put in a micro tube (ϕ13 × 49 mm) with a screw cap and ball-milled for 10 min, during which time the container should be opened two or three times to facilitate solvent release. IR (neat): 2217, 1620, 1420, 1207, 921, 838 cm^{-1}. ^{1}H NMR [400 MHz, THF-d_8, Fig. S13, δ (ppm)]: 8.14 (s, 4H). Anal. Calcd for $C_{18}H_4Au_2N_4F_8$: C, 26.30, H, 0.49; N, 6.81. Found: C, 26.39; H, 0.60; N, 6.79.

Preparation of 2O:

For preparation of **2O**, **2Y** was ground in a ball-mill at 4600 rpm for 5 min. IR (neat): $\tilde{\nu}$ = 2204, 1620, 1421, 1201, 916, 829 cm^{-1}. ^{1}H NMR [400 MHz, THF-d_8, Fig. S14, δ (ppm)]: 8.14 (s, 4H). Anal. Calcd for $C_{18}H_4Au_2N_4F_8$: C, 26.30, H, 0.49; N, 6.81. Found: C, 26.23; H, 0.64; N, 6.63.

Acknowledgements

This work was financially supported by the Funding Program for Next Generation World-Leading Researchers (NEXT Program, No. G002) from the Japan Society for the Promotion of Science (JSPS), the MEXT (Japan) program "Strategic Molecular and Materials Chemistry through Innovative Coupling Reactions" of Hokkaido University, and JSPS KAKENHI Grant-in-Aid for Young Scientists (B), 26810042. We also thank for supports of Frontier Chemistry Center Akira Suzuki "Laboratories for Future Creation" Project.

Notes and references

[a] Division of Chemical Process Engineering and Frontier Chemistry Center (FCC), Graduate School of Engineering, Hokkaido University, Sapporo, Hokkaido, 060-8628, Japan

[b] Catalysis Research Center, Hokkaido University, Sapporo, Hokkaido, 001-0021, Japan

[c] Department of Chemistry and Materials Science, Graduate School of Tokyo Institute of Technology, Meguro-ku, Tokyo, 152-8551, Japan

† Electronic Supplementary Information (ESI) available: X-ray crystallographic data, optical properties, characterization and

interconversion of **2B**, **2G**, **2Y**, and **2O**, and other additional information. See DOI: 10.1039/b000000x/.

1 (a) Z. Chi, X. Zhang, B. Xu, X. Zhou, C. Ma, Y. Zhang, S. Liu and J. Xu, *Chem. Soc. Rev.*, 2012, **41**, 3878–3896; (b) X. Zhang, Z. Chi, Y. Zhang, S. Liu and J. Xu, *J. Mater. Chem. C*, 2013, **1**, 3376–3390; (c) Y. Sagara and T. Kato, *Nat. Chem.*, 2009, **1**, 605–610; (d) A. L. Balch, *Angew. Chem. Int. Ed.*, 2009, **48**, 2641–2644; (e) C. Jobbágy and A. Deák, *Eur. J. Inorg. Chem.*, 2014, **2014**, 4434–4449

2 Y. Sagara and T. Kato, *Angew. Chem. Int. Ed.*, 2011, **50**, 9128–9132.

3 Z. Ma, M. Teng, Z. Wang, S. Yang and X. Jia, *Angew. Chem. Int. Ed.*, 2013, **52**, 12268–12272.

4 K. Nagura, S. Saito, H. Yusa, H. Yamawaki, H. Fujihisa, H. Sato, Y. Shimoikeda and S. Yamaguchi, *J. Am. Chem. Soc.*, 2013, **135**, 10322–10325.

5 S. Yagai, S. Okamura, Y. Nakano, M. Yamauchi, K. Kishikawa, T. Karatsu, A. Kitamura, A. Ueno, D. Kuzuhara, H. Yamada, T. Seki and H. Ito, *Nat. Commun.*, 2014, **5**, 4013.

6 (a) H. Ito, T. Saito, N. Oshima, N. Kitamura, S. Ishizaka, Y. Hinatsu, M. Wakeshima, M. Kato, K. Tsuge and M. Sawamura, *J. Am. Chem. Soc.*, 2008, **130**, 10044–10045; (b) K. Kawaguchi, T. Seki, T. Karatsu, A. Kitamura, H. Ito and S. Yagai, *Chem. Commun.* 2013, **49**, 11391–11393; (c) N. D. Nguyen, G. Zhang, J. Lu, A. E. Sherman and C. L. Fraser, *J. Mater. Chem.*, 2011, **21**, 8409–8415; (d) S. H. Lim, M. M. Olmstead and A. L. Balch, *Chem. Sci.*, 2013, **4**, 311–318; (e) H. Sun, S. Liu, W. Lin, K. Y. Zhang, W. Lv, X. Huang, F. Huo, H. Yang, G. Jenkins, Q. Zhao and W. Huang, *Nat. Commun.*, 2014, **5**, 3601; (f) W. Li, L. Wang, J.-P. Zhang and H. Wang, *J. Mater. Chem. C* 2014, **2**, 1887–1892; (g) M. S. Kwon, J. Gierschner, J. Seo and S. Y. Park, *J. Mater. Chem. C*, 2014, **2**, 2552–2557.

7 (a) B.-C. Tzeng, T.-Y. Chang, and H.-S. Sheu, *Chem. Eur. J.* 2010, **16**, 9990–9993; (b) J. Ni, X. Zhang, N. Qiu, Y. H. Wu, L. Y. Zhang, J. Zhang and Z. N. Chen, *Inorg. Chem.*, 2011, **50**, 9090–9096; (c) S. J. Choi, J. Kuwabara, Y. Nishimura, T. Arai and T. Kanbara, *Chem. Lett.* 2012, **41**, 65–67; (d) N. Zhao, Z. Yang, J. W. Lam, H. H.; Sung, N. Xie, S. Chen, H. Su, M. Gao, I. D. Williams, K. S. Wong and B. Z. Tang, *Chem. Commun.*, 2012, **48**, 8637–8639; (e) A. Han, P. Du, Z. Sun, H. Wu, H. Jia, R. Zhang, Z. Liang, R. Cao and R. Eisenberg, *Inorg. Chem.*, 2014, **53**, 3338–3344; (f) C. Jobbágy, M. Molnár, P. Baranyai, A. Hamza, G. Pálinkás and A. Deák, *CrystEngComm*, 2014, **16**, 3192–3202; (g) J. Ni, Y.-G. Wang, H.-H. Wang, Y.-Z. Pan, L. Xu, Y.-Q. Zhao, X.-Y and Liu, J.-J. Zhang, *Eur. J. Inorg. Chem.*, 2014, **2014**, 986–993; (h) J.; Ni, Y.-G. Wang, H.-H. Wang, L. Xu, Y.-Q. Zhao, Y.-Z. Pan and J.-J. Zhang, *Dalton Trans.*, 2014, **43**, 352–360; (i) X.-C. Shan, F.-L. Jiang, L. Chen, M.-Y. Wu, J. Pan, X.-Y. Wan and M.-C. Hong, *J. Mater. Chem. C*, 2013, **1**, 4339–4349; (j) X. Zhou, H. Li, Z. Chi, X. Zhang, J. Zhang, B. Xu, Y. Zhang, S. Liu and J. Xu, *New J. Chem.*, 2012, **36**, 685–693.

8 (a) N. Harada, Y. Abe, S. Karasawa and N. Koga, *Org. Lett.*, 2012, **14**, 6282–6285; (b) N. Harada, S. Karasawa, T. Matsumoto and N. Koga, *Cryst. Growth Des.*, 2013, **13**, 4705–4713; (c) S.-J. Yoon, J. W. Chung, J. Gierschner, K. S. Kim, M.-G. Choi, D. Kim and S. Y. Park, *J. Am. Chem. Soc.*, 2010, **132**, 13675–13683; (d) M.-S. Yuan, D.-E. Wang, P. Xue, W. Wang, J.-C. Wang, Q. Tu, Z. Liu, Y. Liu, Y. Zhang and J. Wang, *Chem. Mater.*, 2014, **26**, 2467–2477; (e) J. Kunzelman, M. Kinami, B. R. Crenshaw, J. D. Protasiewicz and C. Weder, *Adv. Mater.*, 2008, **20**, 119–122.

9 (a) T. Seki, K. Sakurada and H. Ito, *Angew. Chem. Int. Ed.*, 2013, **52**, 12828–12832; (b) H. Ito, M. Muromoto, S. Kurenuma, S. Ishizaka, N. Kitamura, H. Sato and T. Seki, *Nat. Commun.*, 2013, **4**, 2009.

10 (a) K. Fujii, Y. Ashida, H. Uekusa, F. Guo and K. D. M. Harris, *Chem. Comm.*, 2010, **46**, 4264–4266. (b) K. Fujii, H. Uekusa, N. Itoda, G. Hasegawa, E. Yonemochi, K. Terada, Z. Pan and K. D. M. Harris, *J. Phys. Chem. C*, 2010, **114**, 580–586. (c) K. Fujii, H. Uekusa, N. Itoda, E. Yonemochi and K. Terada, *Cryst. Growth Des.*, 2012, **12**, 6165–6172. (d) K. Fujii, M. Aoki and H. Uekusa, *Cryst. Growth Des.*, 2013, **13**, 2060–2066.

11 (a) A. L. Balch, *Gold Bull.*, 2004, **37**, 45–50; (b) P. Pyykko, *Angew. Chem. Int. Ed.*, 2004, **43**, 4412–4456; (c) V. W. Yam and E. C. Cheng, *Chem. Soc. Rev.*, 2008, **37**, 1806–1813; (d) M. J. Katz, K. Sakai and D. B. Leznoff, *Chem. Soc. Rev.*, 2008, **37**, 1884–1895; (e) H. Schmidbaur and A. Schier, *Chem. Soc. Rev.*, 2008, **37**, 1931–1951; (f) X. He and V. W.-W. Yam, *Coord. Chem. Rev.*, 2011, **255**, 2111–2123; (g) H.; Schmidbaur and A. Schier, *Chem. Soc. Rev.*, 2012, **41**, 370–412.

12 Actually, direct evidence of the aurophilic interaction of **1Y** has not been obtained even by EXAFS study measured at 4 K. The peak assignable to Au···Au distance of **1Y** was found around at 5 Å, which corresponded to the Au···Au distance of unground **1B**. This result may be caused by the only small amount of the aurophilic interactions in **1Y**, so that even EXAFS study could not observe the aurophilic interactions. The more detailed discussion will be reported elsewhere.

13 Addition of other solvents, like dichloromethane, chloroform, cyclohexanone and dimethoxyethane, induces various emission color changes of **2**. For example, chloroform addition to **2G** provided red-emitting powder which shows emission spectrum peaked at 645 nm. Unfortunately, we can not determine, at present, detailed molecular arrangements of the resulting materials, and thus these behaviors will be discussed elsewhere. Moreover, recrystallization of **2** from cyclohexanone, THF, and dimethoxyethane (maximum solubility c_{max} > 0.1 mg/mL) afforded the yellow-emitting solid (similar to **2Y**). Since **2** can not solvate these solvents, it is proposed that non-solvated **2Y** was formed under this condition.

14 **2Y** is also transformed to **2B** upon addition of acetone.

15 (a) J. Bernstein, *Polymorphism in molecular crystals*; Clarendon Press/International Union of Crystallography, 2002; Vol. 14; (b) Y. Mnyukh, *Fundamentals of Solid-State Phase Transitions: Ferromagnetism and Ferroelectricity*; Authorhouse, 2001.

16 Residual electron density in 1-D channel is estimated to be seventeen electrons per unit cell. This is corresponding to 0.5 equivalents for acetone and/or 2 equivalents for water. ^{1}H NMR spectrum of **2G** confirms that both acetone and H_2O could be present (Fig. S12†).

17 D. Yan, G. Fan, Y. Guan, Q. Meng, C. Li and J. Wang, *Phys. Chem. Chem. Phys.*, 2013, **15**, 19845–19852.

18 A diffraction peak at 6.6° is derived from residual **2G** phase contaminated within **2Y** phase. See also Fig. 7c.

19 For an example of PXRD measurements and the Rietveld refinement technique for the study of the crystalline size of the ground phase of mechanochromic compounds rather than full structure analysis, see: S. Perruchas, X. F. Le Goff, S. Maron, I. Maurin, F. Guillen, A.

Garcia, T. Gacoin and J. P. Boilot, *J. Am. Chem. Soc.*, 2010, **132**, 10967–10969.

20 The **2Y** phase thermally transformed from **2G** can not further transform to **2O** phase upon phase transition; whereas mechanically prepared **2Y** shows transformation into **2O** phase. This result indicates that preparation methods of **2Y** phase affect its phase transition behaviors.

21 As mentioned above, any solvent molecules do not exist in the crystalline lattice of **2Y** based on thermal analyses, elemental analyses and ^{1}H NMR and IR spectroscopy (Fig. 8, S13 and S15 and Table S4†).

22 DSC analysis of **2B** was not performed because it is unstable without acetone.

23 This discussion is agreed well with the fact that the as-synthesized form of **2** is principally similar to **2Y** as shown in their PXRD pattern (Fig. 6), likely because a metastable form **2Y** is kinetically trapped.